Journal of Metals, Materials and Minerals, 36(4), e2685, 2026

Enhanced energy-storage performance and electric-field-induced strain in Ta-doped $(Bi_{0.465}Na_{0.465}Ba_{0.07})TiO_3$ lead-free ceramics

Pathit PREMWICHIT[1], Theerawat LUNTHAIYO[1], Onthida KOSASANG[2], and Sasipohn PRASERTPALICHAT[1,3,*]

[1] *Department of Physics, Faculty of Science, Naresuan University, Phitsanulok 65000, Thailand*
[2] *Center of Innovative Materials for Sustainability (iMatS), School of Science, Mae Fah Luang University, Thailand*
[3] *Research Center for Academic Excellence in Applied Physics, Faculty of Science, Naresuan University, Phitsanulok 65000, Thailand*

***Corresponding author e-mail**: sasipohnp@nu.ac.th

Received date:
31 March 2026
Revised date:
2 April 2026
Accepted date:
14 May 2026

Keywords:
Environmentally friendly ceramics;
Ta substitution;
Energy-storage capability;
Relaxor behavior

Abstract

The influence of Ta^{5+} substitution on lead-free $(Bi_{0.465}Na_{0.465}Ba_{0.07})Ta_xTi_{(1-x)}O_3$ (BNBT–xTa, x = 0.0 to 0.03) ceramics was investigated. The samples were prepared using a conventional solid-state route, resulting in a phase-pure perovskite structure with pseudocubic characteristics for all compositions. With increasing Ta content, the electrical response gradually shifted toward relaxor behavior, as indicated by slimmer *P*–*E* loops, reduced remanent polarization, and a shift of T_s toward lower temperatures. This transition was also reflected in the strain characteristics, where *S*–*E* loops evolved from typical butterfly shapes to sprout-like profiles. The sample with x = 0.01 showed the best strain performance, reaching ~0.23% strain along with a normalized coefficient of ~383 pm·V^{-1}. Energy-storage performance was significantly improved, with a maximum W_{rec} of ~0.90 J·cm^{-3} for x = 0.02, while efficiency further increased to 68% for x = 0.03. In parallel, electrical resistivity increased by nearly an order of magnitude, accompanied by a rise in activation energy from 1.53 eV to 1.71 eV, suggesting suppressed charge transport due to enhanced energy barriers. Overall, Ta^{5+} substitution effectively tailors both electrical and electromechanical properties, making BNBT-based ceramics promising candidates for advanced lead-free capacitor applications and actuators.

1. Introduction

Growing interest in environmentally friendly functional materials has driven extensive research toward replacing conventional lead-based piezoelectric ceramics. Among these, $Pb(Zr_{1-x}Ti_x)O_3$ has long been recognized for its superior electromechanical performance, particularly in the vicinity of the morphotropic phase boundary (MPB) [1–4]. However, concerns associated with lead toxicity and PbO volatilization during high-temperature processing have led to increasingly strict regulations, motivating the pursuit of alternative lead-free compositions [5].

In this context, $(Bi_{0.5}Na_{0.5})TiO_3$ (BNT) is considered a promising candidate owing to its relatively high polarization and elevated Curie temperature. Despite these advantages, its practical application is hindered by intrinsic limitations, such as a high coercive field and significant dielectric loss. To overcome these drawbacks, compositional modification through solid-solution formation has been widely employed [6]. A well-known approach involves combining BNT with $BaTiO_3$ (BT) to form the BNT–BT system, where enhanced functional properties can be achieved near a critical composition range (i.e., the MPB around x = 0.06 to 0.07) [7,8]. In particular, the system exhibits a coexistence of rhombohedral and tetragonal phases over this composition range gives rise to improved dielectric and piezoelectric responses. Nevertheless, even with such modifications, issues related to relatively large remanent polarization and suboptimal energy-storage efficiency remain, limiting the functional performance of BNT-derived ceramics in high-energy-density capacitor applications [9,10].

Chemical modification has been widely explored as an effective approach for enhancing the properties of BNT–BT ceramics. Common approaches include forming solid solutions with other ABO_3-type perovskites as well as introducing donor dopants, similar to those employed in PZT systems, at both A- and B-sites [11]. In particular, donor doping has been shown to facilitate the development of relaxor phases and enhance multiple functional properties, such as dielectric response, ferroelectric behavior, strain response under an applied electric field, along with energy storage capability [12-14]. For instance, Bafandeh *et al.* [15] incorporated $(Ga_{0.5}Ta_{0.5})^{4+}$ into 0.93BNT–0.07BT, which induces a transition from a ferroelectric state to an ergodic relaxor phase near room temperature. At BNBT-3GT, a relatively large unipolar strain of ~0.40% was observed under an applied field of 60 kV·cm^{-1}, accompanied by a high normalized strain of 667 pm·V^{-1}. These findings demonstrate that Ga/Ta co-doping is an efficient approach for improving the electrostrain behavior of BNBT-based ceramics. Similarly, Xu *et al.* [16] studied Ta-modified 0.94BNT–0.06BT ceramics, where Ta incorporation promoted the stabilization of a relaxor antiferroelectric phase and induced double *P*–*E* loops. At x = 0.02, the maximum recoverable energy density (W_{rec}) reached ~0.94 J·cm^{-3} under an applied field of 60 kV·cm^{-1}, together with improved efficiency and good thermal stability up to 120°C. In addition,

Ta doping led to finer grains and lower remanent polarization, further confirming its effectiveness in enhancing energy-storage properties in BNT–BT systems. Previous studies have indicated that tantalum (Ta^{5+}) can significantly influence lattice structure and domain behavior [16]. It has also been reported that Ta incorporation improves relaxor characteristics and leads to slimmer *P–E* hysteresis loops, which is beneficial for energy-storage applications [17]. Despite these advances, investigations on BNT–*x*BT ceramics near the MPB region ($x \approx 0.07$) produced through a standard solid-state process remain relatively limited. Therefore, this study aims to clarify the role of Ta^{5+} substitution in $(Bi_{0.465}Na_{0.465}Ba_{0.07})Ta_xTi_{(1-x)}O_3$ ceramics prepared via a solid-state method. Attention is given to their structural, microstructural, dielectric, ferroelectric, piezoelectric, resistive, and activation energy characteristics, as well as their energy-storage performance.

2. Experimental procedure

BNBT–*x*Ta ceramics with nominal compositions of $(Bi_{0.465}Na_{0.465}Ba_{0.07})Ta_xTi_{(1-x)}O_3$ were fabricated using a conventional solid-state route. The starting materials included $BaCO_3$, Na_2CO_3, Bi_2O_3, TiO_2, and Ta_2O_5 powders, all with purities above 99%, obtained from commercial suppliers such as Sigma-Aldrich and Alfa Aesar. The raw powders were first weighed according to the stoichiometric ratios of the target composition, then dispersed in ethanol and wet-milled for 24 h using zirconia media to ensure homogeneous mixing. After removal of the solvent, the dried mixtures were calcined at 800°C for 2 h. The calcined powders were subsequently milled again to improve compositional uniformity further. A binder (polyvinyl butyral, 3 wt%) was added prior to shaping, and the powders were pressed into disc-shaped pellets with diameters of approximately 10 mm and thicknesses of ~1.2 mm. To suppress the evaporation of volatile elements such as Bi and Na during sintering, the pellets were embedded in sacrificial powder and placed in a covered crucible. Binder burnout was carried out at 400°C for 3 h, followed by sintering at 1175°C for 2 h in air.

The phase constitution of the sintered ceramics was examined by X-ray diffraction over a 2θ range of 20° to 80°. The bulk density was determined using the Archimedes method. For microstructural analysis, the specimen surfaces were mechanically polished and subsequently thermally etched at a temperature approximately 100°C below the sintering temperature for 30 min, followed by observation using field-emission scanning electron microscopy (FESEM, Apreo S). Prior to electrical characterization, the samples were polished down to a thickness of ~0.6 mm to 0.9 mm and coated with silver electrodes on both surfaces. The electrodes were then heat-treated at 700°C for 30 min to improve electrical contact. Dielectric properties were evaluated using an LCR meter over a frequency range of 1 kHz to 100 kHz within a temperature interval of 30°C to 450°C. The polarization–electric field (*P–E*) and strain–electric field (*S–E*) hysteresis loops were measured at room temperature using a Premier II ferroelectric tester operated at 1 Hz. Impedance spectroscopy was carried out in air over a temperature range of 480°C to 560°C, covering frequencies from 1 Hz to 10 MHz. In addition, UV–Vis–NIR absorption spectra were recorded at ambient conditions using a UV–Vis–NIR spectrophotometer to estimate the optical bandgap.

3. Results and discussion

Figure 1 shows the X-ray diffraction patterns obtained within a 2θ range of 20° to 80° for powders obtained from crushed BNBT–*x*Ta ($x = 0.0$ to 0.03) ceramics. All samples display a single-phase perovskite structure with no detectable secondary phases. Closer examination of the diffraction peaks associated with the (111) and (200) planes indicates well-defined and symmetric reflections located at approximately $2\theta \approx 39.7°$ and 46.5°, respectively, confirming the formation of a pseudo cubic structure [18]. Furthermore, a gradual displacement of the diffraction peaks toward lower 2θ angles is evident with increasing Ta^{5+} content, suggesting lattice expansion. This trend is likely related to the substitution of Ti^{4+} ions by the relatively larger Ta^{5+} ions (Ta^{5+}: 0.64 Å; Ti^{4+}: 0.605 Å) within the B-site positions of the perovskite lattice [19].

Figure 2(a–d) show the thermally etched microstructures for BNBT–*x*Ta ceramics with $x = 0.0$–0.03. The bulk density, as measured by the Archimedes technique, rises from 5.40 g·cm^{-3} for $x = 0$ to 5.45 g·cm^{-3}, 5.47 g·cm^{-3}, and 5.48 g·cm^{-3} for $x = 0.01$ to 0.03, respectively. The mean grain size was evaluated using the linear intercept method. For the undoped sample ($x = 0.0$), an average grain size of approximately 0.84 μm is observed, along with noticeable porosity. With increasing Ta content, the microstructure becomes more compact and the porosity is reduced. The mean grain size shows a slight reduction to ~0.83 μm (for $x = 0.01$), followed by a pronounced reduction to ~0.63 μm (for $x = 0.02$), as illustrated in Figure 2(c). A subsequent increase to ~0.69 μm is observed for $x = 0.03$, as seen in Figure 2(d). This grain refinement behavior is associated with variations in defect concentrations induced by Ta doping. For BNT-based ceramics, Bi and Na volatilization during elevated-temperature processing typically generates cation vacancies, such as bismuth vacancies (V'''_{Bi}) and sodium vacancies (V'_{Na}), together with oxygen vacancies ($V^{\bullet\bullet}_{O}$), as described by Equation (1) and Equation (2) [20].

$$2Bi^{X}_{Bi} + 3O^{X}_{O} \rightarrow 2V'''_{Bi} + 3V^{\bullet\bullet}_{O} + Bi_2O_3 \quad (1)$$

$$2Na^{X}_{Na} + O^{X}_{O} \rightarrow 2V'_{Na} + V^{\bullet\bullet}_{O} + Na_2O \quad (2)$$

Upon donor doping with Ta_2O_5, oxygen vacancies can be compensated, resulting in a decreased concentration of oxygen vacancies, as represented in Equation (3).

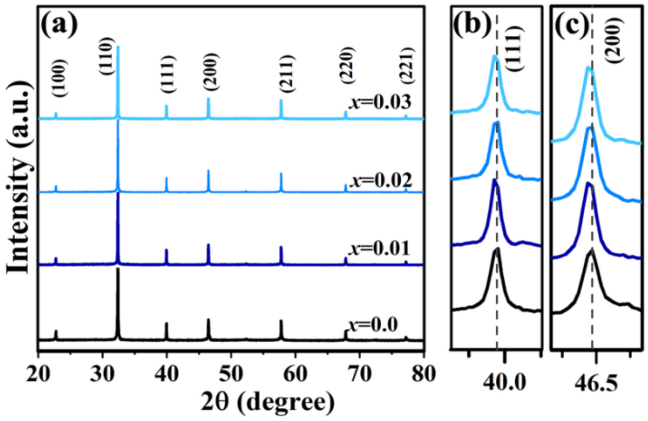

Figure 1. Diffraction patterns obtained using XRD for BNBT–*x*Ta ($x = 0.0$ to 0.03) ceramics. Panel (a) shows the full scan over $2\theta = 20°$ to 80°, while (b) and (c) highlight enlarged regions near ~39.9° and 46° to 47°, respectively.

$$Ta_2O_5 + V_O^{\bullet\bullet} \xrightarrow{2TiO_2} 2Ta_{Ti}^{\bullet} + 5O_O^X \quad (3)$$

It is well established that oxygen vacancies facilitate grain growth during sintering [21]. Therefore, the reduction of oxygen vacancy concentration suppresses grain growth, leading to finer grain sizes with increasing Ta^{5+} content. Such behavior is consistent with previous observations in BNT-based ceramics modified with other donor dopants [22–24].

The temperature-dependent dielectric behavior of unpoled BNBT–xTa with x = 0.0 to 0.03 compositions was examined over 30°C to 450°C at selected frequencies of 1 kHz, 10 kHz, and 100 kHz (see Figure 3(a–d)). For all compositions, the ε and tanδ responses exhibit two characteristic features. At lower temperatures, a weak and frequency-dispersive shoulder (T_s) can be observed, while a more pronounced peak appears at higher temperatures, which corresponds to the temperature of maximum dielectric permittivity (T_m). These two features are closely linked to changes in polar nanoregions and phase changes between rhombohedral (*R3c*) and tetragonal (*P4bm*) symmetries. The T_s feature is generally associated with the onset of local structural rearrangement, whereas the T_m peak reflects the dominant phase transition behavior associated with stabilization of *P4bm* phase [25]. With increasing Ta^{5+} concentration, the T_s temperature progressively shifts toward lower values, decreasing from ~150°C for x = 0.0 to 114, 89, and 84°C when x = 0.01 to 0.03 (Table 1). Simultaneously, the dielectric constant shows an overall decrease, accompanied by noticeable peak broadening around T_m, indicating an enhancement of relaxor characteristics [26–30]. In addition, dielectric loss (tanδ) in the high-temperature region (>350°C) is markedly reduced as Ta content increases. Such a reduction in dielectric loss may be attributed to suppression of space charge effects, mainly due to a lower concentration of oxygen vacancies ($V_O^{\bullet\bullet}$) and other mobile charge carriers within the material [31].

To further understand the influence of Ta^{5+} substitution on electrical transport behavior, impedance spectroscopy (IS) was employed for BNBT–xTa (x = 0.0 to 0.03) ceramics. Measurements were carried out over 480°C to 560°C under frequencies spanning 1 Hz to 10 MHz, and the resulting complex impedance spectra ($Z^* = Z'$ vs. Z'') for all compositions are presented in Figure 4(a–d). Each composition exhibits a single semicircular arc, indicating that the electrical response is predominantly governed by the bulk contribution [32]. With increasing temperature, the impedance spectra of all compositions gradually transform from a distorted semicircular arc into a smaller and more symmetric one. Such behavior is characteristic of negative temperature coefficient resistance, commonly found in semiconducting materials and BNT-based systems [33-35]. This phenomenon originates from the thermally activated motion of weakly trapped charge carriers [36].

The resistivity (ρ) of BNBT–xTa (x = 0.0, 0.01, 0.02, and 0.03) ceramics at 540°C was calculated from Z'' vs f inset plots in Figure 4(e), using the relation $R = 2Z''_{max}$, where R represents the resistance and Z''_{max} corresponds to the peak magnitude of the imaginary impedance component. For the undoped composition (x = 0.0), the resistivity was 8.40×10^5 Ω·cm. As the Ta content increases, the resistivity increases significantly to 2.57×10^6 Ω·cm for x = 0.03, representing nearly a tenfold increase. This enhancement in resistivity is mainly associated with reduced oxygen vacancy concentration, as described in Equation (2). This effect is attributed to Ta incorporation, which effectively limits the formation of oxygen vacancies during heat treatment at elevated temperatures. Consequently, the reduced defect concentration leads to fewer mobile charge carriers and thus higher resistivity. This trend aligns with findings in previous studies [24,37,38]. Moreover, this increase in resistivity is correlated with a decrease in dielectric loss at temperatures above 350°C, a desirable property for enhancing dielectric ceramic performance [32,39].

To determine the activation energy (E_a) for electrical conductivity, the natural logarithm of electrical conductivity (ln σ) was plotted against the inverse temperature (1000/T) for BNBT–xTa with x = 0.0, 0.01, 0.02, and 0.03 compositions (see Figure 4(f)), [40]:

$$\sigma = \sigma_0 \exp\left(\frac{-E_a}{k_B T}\right) \quad (4)$$

where σ corresponds to electrical conductivity, σ_0 denotes the pre-exponential term, k_B is the Boltzmann constant, and T refers to absolute temperature.

The extracted E_a for BNBT–xTa ceramics was found to be approximately 1.53 eV for x = 0.0, which agrees well with previously reported values for BNT-based materials. This value is approximately half of the bandgap typically reported for BNT-based systems (E_g ≈ 3.0 eV to 3.5 eV), implying that charge transport is dominated by an intrinsic conduction mechanism involving thermally activated carriers [41]. As the Ta content increases (x = 0.01 to 0.03), the activation energy gradually rises from 1.58 eV to 1.71 eV, suggesting an increased energy barrier is required for charge carrier migration. This results in reduced electrical conductivity [42]. This trend is consistent with the experimentally observed increase in resistivity. Additionally, the increase in E_a with higher Ta content can be attributed to a decrease in oxygen vacancy concentration [43,44], as explained in Equation (3). The combined increase in resistivity and activation energy is expected to promote better electromechanical coupling in the material.

The optical bandgap (E_g) of BNBT–xTa with compositions of x = 0.0 to 0.03 was estimated from UV–Vis absorption spectra (see Figure 4(g)) using the Kubelka–Munk approach [45], expressed as $(F(R)hv)^n = A(hv–E_g)$. Here, $F(R)$denotes the Kubelka–Munk transformation, while hv corresponds to photon energy and A is a scaling constant. The parameter depends on the electronic transition type, where values of 1/2 and 2 are typically associated n with direct and indirect allowed transitions, respectively, whereas 3/2 and 3 correspond to forbidden transitions. In this study, n=2 was selected, and a slight reduction in E_g was observed with increasing Ta content. Specifically, E_g decreases from 3.26 eV at x = 0.0 to approximately 3.13 eV, 3.11 eV, and 3.12 eV for x values of 0.01 to 0.03**.** The variation in bandgap is relatively small (~4.60%) and remains within a narrow range. The slight reduction in E_g may arise from changes in the electronic structure of the material due to Ta doping, potentially associated with the formation of defect states or shifts in energy levels within the bandgap, influencing the behavior of electrons in the crystal [46]. In particular, compared with systems containing high dopant concentrations where extensive defect accumulation can lead to pronounced bandgap narrowing, the small reduction in E_g observed in this work indicates that the bandgap narrowing induced by low Ta^{5+} doping remains insignificant [46–48].

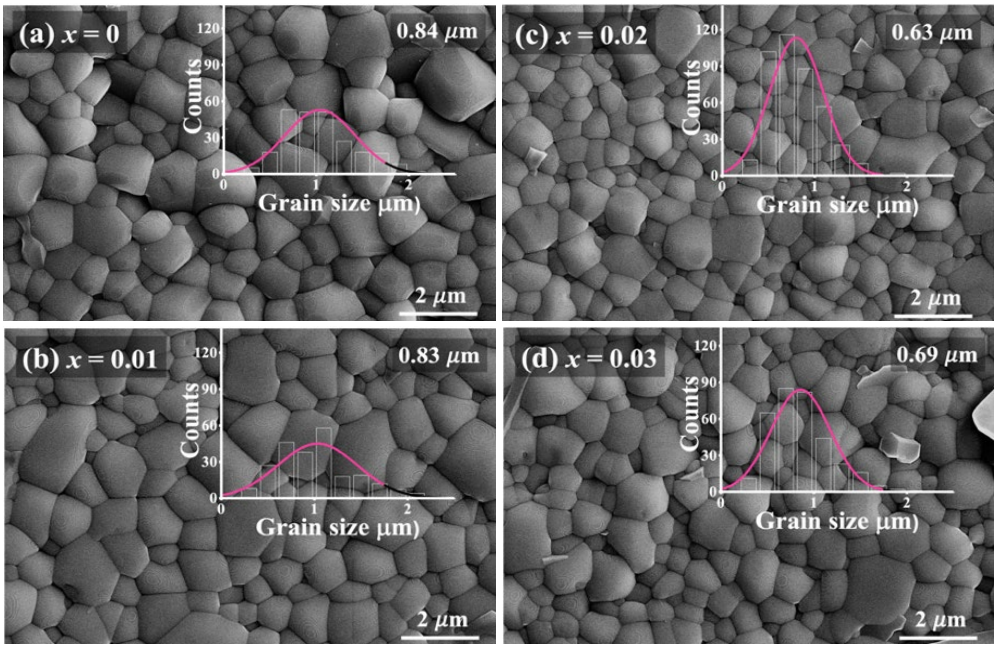

Figure 2. (a)–(d) Thermally etched morphologies for BNBT–*x*Ta compositions (x = 0.0 to 0.03) obtained following heat treatment at 1075°C for 30 min. Grain size distributions corresponding to each sample are shown as inset images.

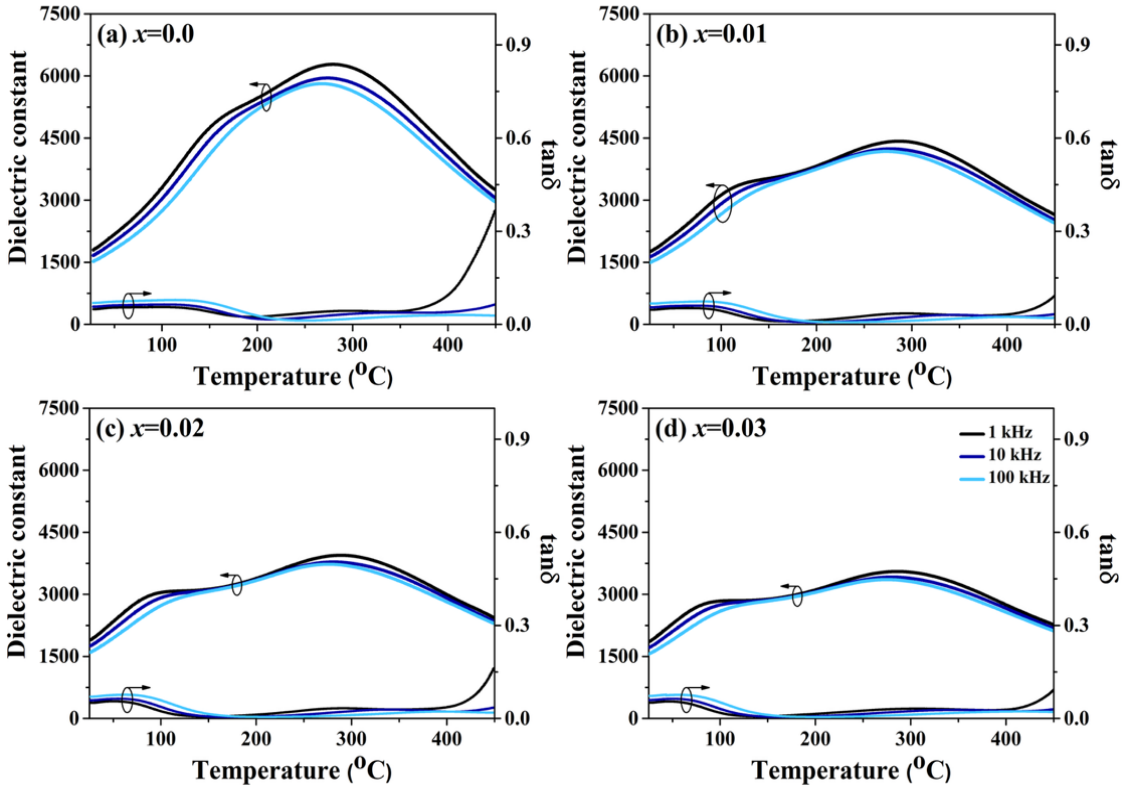

Figure 3. (a)–(d) Dielectric behavior as a function of temperature of unpoled BNBT–*x*Ta (x = 0.0 to 0.03) ceramics, including ε and tanδ, measured between 30°C and 450°C at representative frequencies of 1 kHz to 100 kHz.

Table 1. Summary of dielectric parameters (T_s, T_m, ε_r, ε_m, tanδ_r, tanδ_m) for BNBT–*x*Ta (x = 0.0 to 0.03) ceramics.

Compositions	T_s [°C]	T_m [°C]	ε_r	tanδ_r	ε_m	tanδ_m
x = 0.0	150	278	1876	0.049	6279	0.043
x = 0.01	114	271	2144	0.057	5581	0.023
x = 0.02	89	280	2085	0.072	5360	0.018
x = 0.03	84	289	2303	0.079	4409	0.033

Table 2. Summary of energy-storage performance and strain response for BNBT–*x*Ta ceramics (*x* = 0 to 0.03).

Compositions	P_r [μC·cm^{-2}]	P_{max} [μC·cm^{-2}]	W [J·cm^{-3}]	W_{rec} [J·cm^{-3}]	η [%]	S_{neg} [%]	S_{max} [%]	d^*_{33} [pm·V^{-1}]
x = 0.0	29.53	37.63	0.46	0.23	50	0.13	0.17	283
x = 0.01	7.58	31.27	1.66	0.85	51	0	0.23	383
x = 0.02	4.13	23.02	1.45	0.90	62	0	0.11	183
x = 0.03	1.99	17.30	1.28	0.88	68	0	0.07	116

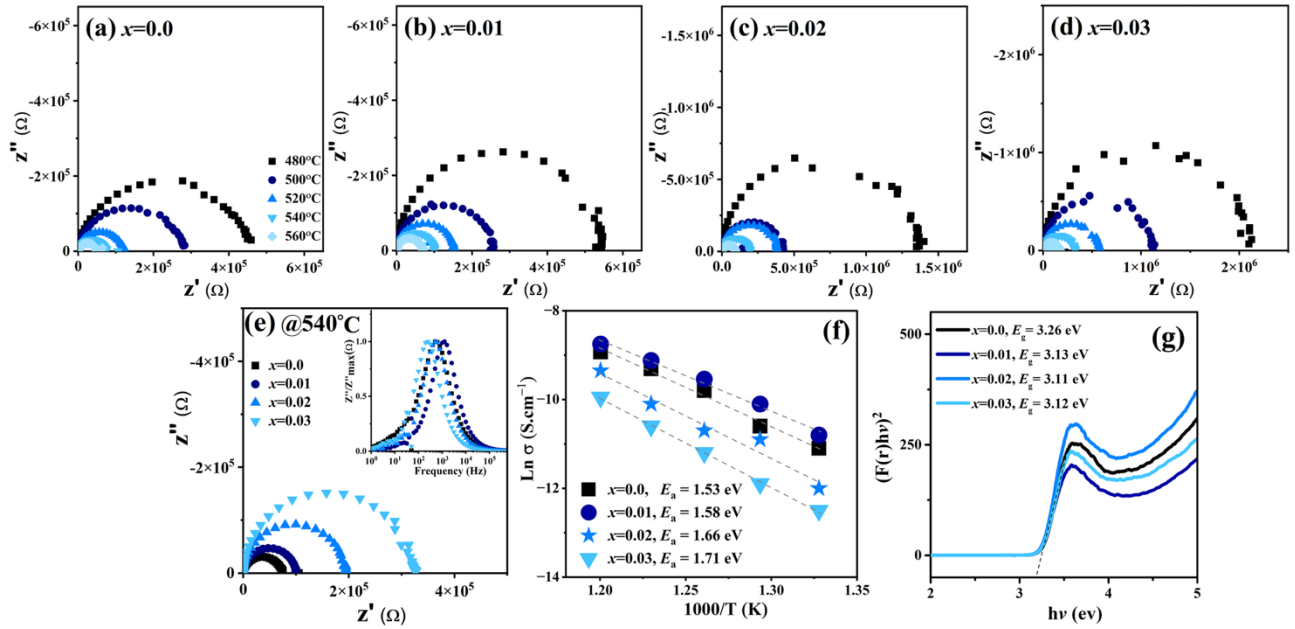

Figure 4. (a–d) Impedance complex-plane representations (Z′–Z″) for BNBT–*x*Ta with *x* ranging from 0 to 0.03 ceramics recorded over 480°C to 560°C. (e) *Z** spectra with inset Z″ vs frequency (*f*) plots at 540°C, (f) Arrhenius plots (ln σ vs 1000/T) with activation energy (E_a), and (g) Optical bandgap values determined based on the Kubelka–Tauc approach.

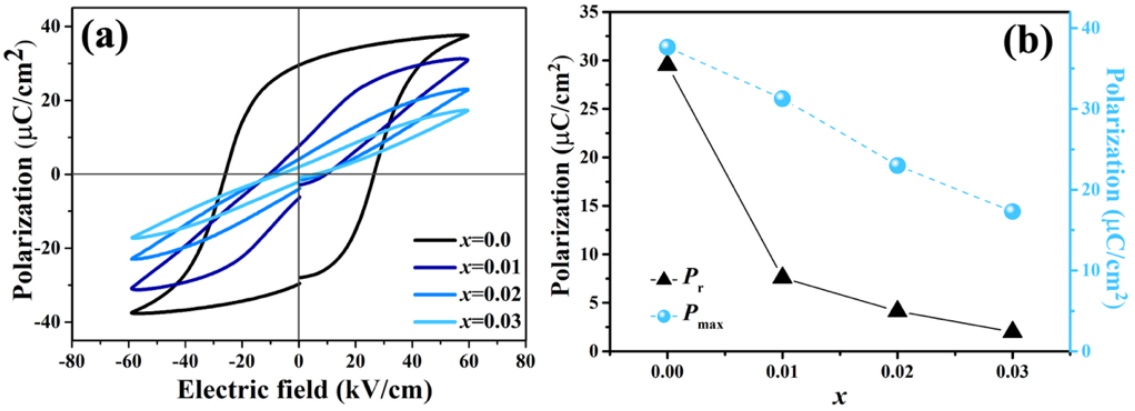

Figure 5. (a–b) Representative polarization–electric field loops obtained for BNBT–*x*Ta compositions (*x* = 0.0 to 0.03) under a driving field of 60 kV·cm^{-1} at ambient temperature.

The bipolar polarization–electric field (*P*–*E*) response of BNBT–*x*Ta with *x* = 0.0 to 0.03 compositions was analyzed at ambient conditions under an electric field of 60 kV·cm^{-1}, as illustrated in Figure 5(a–b). The undoped sample (*x* = 0) displays a distinct square-like hysteresis loop, accompanied by a relatively high coercive field ($E_c \approx 21.5$ kV·cm^{-1}) and remanent polarization ($P_r \approx 29.53$ μC·cm^{-2}), reflecting typical ferroelectric characteristics.

This leads to pronounced hysteresis loss and consequently low energy-storage efficiency (η), indicating that pure BNBT is not suitable for energy-storage purposes. With the introduction of Ta^{5+} (*x* = 0.01 to 0.03), a progressive constriction of the *P*–*E* loops is observed, accompanied by a pronounced decrease in P_r, most notably at *x* = 0.02, as illustrated in Figure 5(c–d) and Table 2. Meanwhile, P_{max} declines from 37.63 μC·cm^{-2} at *x* = 0 to 31.27 μC·cm^{-2} at *x* = 0.01, followed by further reductions to 23.02 μC·cm^{-2} and 17.30 μC·cm^{-2} for *x* = 0.02 and 0.03, respectively. These observations suggest that incorporation of Ta^{5+} promotes the emergence of relaxor-like characteristics in BNBT ceramics. This is consistent with the dielectric

behavior discussed earlier, where increasing Ta content leads to a more diffuse dielectric response, manifested through peak broadening and reduced sharpness, together with weakened frequency dispersion near T_m. Such responses are commonly associated with relaxor ferroelectrics and are typically attributed to the disruption of extended ferroelectric domain ordering, giving rise to more constricted polarization–electric field loops [49,50]. The reduction in P_r, along with the variation in P_{max}, contributes significantly to the improvement of energy-storage capability in BNBT–xTa ceramics.

The energy-storage characteristics, specifically the recoverable energy density (W_{rec}) and efficiency (η), were assessed using unipolar polarization–electric field responses, and the corresponding data are presented in Figure 6(a–d) and Table 2. The total energy storage density (W) and W_{rec} are obtained from the integration of the electric field with respect to polarization, expressed as: $W = \int_0^{P_{max}} EdP$, $W_{rec} = \int_{P_r}^{P_{max}} EdP$, $\eta = (W_{rec}/W) \times 100\%$, where the symbols follow the definitions given earlier [51,52]. An overall enhancement in both W_{rec} and η is observed as the Ta content rises. For the undoped composition ($x = 0$), W_{rec} is 0.23 J·cm^{-3} with an efficiency of 50%. Upon introducing Ta ($x = 0.01$), W_{rec} increases significantly to 0.85 J·cm^{-3}, accompanied by a slight improvement in efficiency to 51%. A further increase in Ta concentration to $x = 0.02$ results in the highest W_{rec} of 0.90 J·cm^{-3} and η of 62%, indicating the most favorable energy storage behavior among all studied compositions. At $x = 0.03$, W_{rec} shows a minor decrease to 0.88 J·cm^{-3}, while η continues to increase, reaching 68%. The improvement in efficiency is primarily associated with the reduction in energy loss (W_{loss}). This behavior can be associated with the decrease in P_r and the progressive constriction of the polarization–electric field loops resulting from Ta^{5+} incorporation. These observations are consistent with the dielectric characteristics discussed earlier and together lead to improved energy-storage properties in BNBT–xTa ceramics.

The strain–electric field (S–E) hysteresis behavior of BNBT–xTa with $x = 0.0$ to 0.03 compositions was examined under a driving field of 60 kV·cm^{-1} at ambient conditions. For the undoped sample ($x = 0.0$), a well-defined butterfly-like loop is observed, characterized by a maximum positive strain (S_{max}) of 0.17% and a negative strain (S_{neg}) of 0.13%, as shown in Figure 6(a) and Table 2. As Ta concentration increases, the loop morphology gradually changes from a butterfly-like profile to a sprout-like form, accompanied by the disappearance of S_{neg} at $x \geq 0.01$, suggesting relaxor characteristics [53]. The maximum strain appears at $x = 0.01$, reaching 0.23%, while further increases in Ta content lead to reduced values of 0.11% and 0.07% for $x = 0.02$ and 0.03, respectively. The corresponding results are provided in Figure 7 (b–d) and Table 2. A comparable tendency is found for the normalized piezoelectric coefficient (d^*_{33}), defined as S_{max}/E_{max}. The highest value, 383 pm·V^{-1}, is obtained at $x = 0.01$, followed by a pronounced decline to 183 pm·V^{-1} and 116 pm·V^{-1} with further Ta addition. The simultaneous reduction in both S_{max} and d^*_{33} reflects a composition-dependent evolution of electromechanical behavior, indicating a transition from ferroelectric to relaxor-like characteristics [54,55].

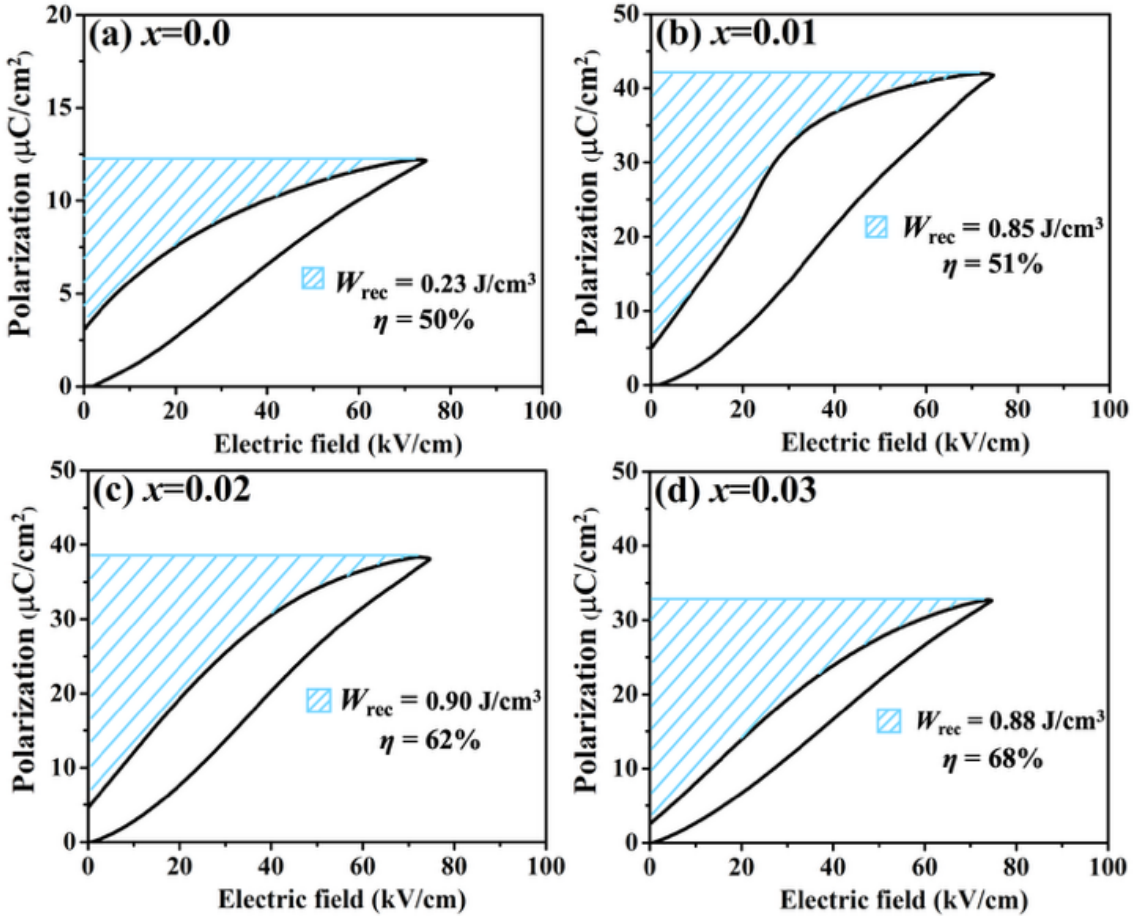

Figure 6. (a–d) Unipolar polarization–electric field characteristics of BNBT–xTa compositions ($x = 0.0$ to 0.03) measured at 75 kV·cm^{-1}, with shaded regions indicating the recoverable energy density (W_{rec}).

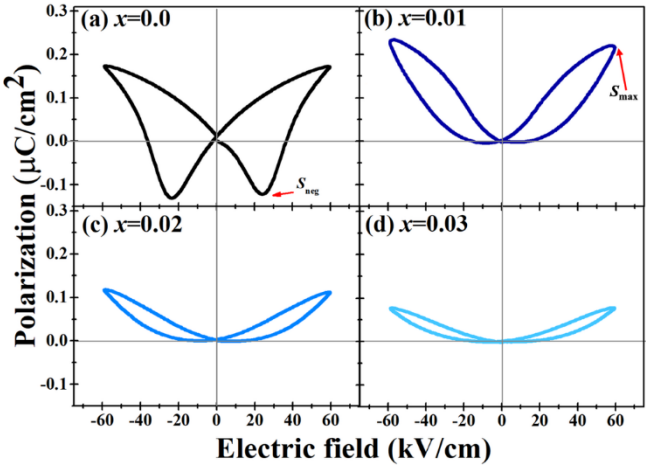

Figure 7. (a–d) Room-temperature *S*–*E* hysteresis characteristics of BNBT–*x*Ta ceramics, illustrating the compositional dependence for $x = 0.0$ to 0.03.

4. Conclusion

In conclusion, $(Bi_{0.465}Na_{0.465}Ba_{0.07})Ta_xTi_{(1-x)}O_3$ compositions within the investigated range ($x \leq 0.03$) were successfully prepared using a standard solid-state route, yielding a single perovskite structure with pseudocubic features. The incorporation of Ta leads to a gradual evolution in electrical response, in agreement with the dielectric characteristics, as reflected by slimmer polarization–electric field loops and reduced remanent polarization. Among the studied samples, the composition at $x = 0.02$ delivers the most balanced performance, exhibiting a recoverable energy density approaching 0.90 $J \cdot cm^{-3}$ together with an energy efficiency of about 62%. In parallel, the strain–electric field behavior undergoes a clear morphological evolution, shifting from a butterfly-like response toward a more sprout-shaped profile as Ta content increases. This evolution is indicative of a progressive change in polarization dynamics, associated with the emergence of relaxor-type characteristics. The composition at $x = 0.01$ shows the highest electromechanical response, with a normalized strain coefficient (d^*_{33}) of approximately 383 $pm \cdot V^{-1}$. Furthermore, the resistivity increases markedly from 8.40×10^5 Ω·cm ($x = 0.0$) to 2.57×10^6 Ω·cm ($x = 0.03$), corresponding to more than an order of magnitude change. This enhancement is associated with a reduction in oxygen vacancy concentration, which limits charge carrier mobility. Meanwhile, the activation energy (E_a) rises from 1.53 eV to 1.71 eV with increasing Ta content, indicating a higher energy barrier for charge transport. Overall, these findings demonstrate that Ta-modified BNBT systems offer a promising pathway toward lead-free materials suitable for high-performance energy-storage and actuator applications.

Acknowledgements

This work was supported by Naresuan University (NU), and National Science, Research and Innovation Fund (NSRF), Grant NO. R2567B075. Partial support was also provided by the Global and Frontier Research University Fund, Naresuan University, Grant NO. R2567C001. The authors would like to express their gratitude to the Department of Physics, Faculty of Science, Naresuan University, for providing research facilities.

References

[1] L. Yang, X. Kong, F. Li, H. Hao, Z. Cheng, H. Liu, J.-F. Li, and S. Zhang, "Perovskite lead-free dielectrics for energy storage applications," *Progress in Materials Science*, vol. 102, pp. 72–108, 2019.

[2] D. Damjanovic, and R. Newnham, "Electrostrictive and piezoelectric materials for actuator applications," *Journal of Intellignet Material Systems and Structures*, vol. 3, no. 2, pp. 190–208, 1992.

[3] J. Lee, S. Hajra, S. Panda, W. Oh, Y. Oh, H. Shin, Y. K. Mishra, and H. J. Kim, "Accelerate the shift to green energy with PVDF based piezoelectric nanogenerator," *International Journal of Precision Engineering and Manufacturing-Green Technology*, vol. 11, no. 1, pp. 233–241, 2024.

[4] R. Guo, L. E. Cross, S.-E. Park, B. Noheda, D. E. Cox, and G. Shirane, "Origin of the high piezoelectric response in $PbZr_{1-x}Ti_xO_3$," *Physical Review Letters*, vol. 84, no. 23, pp. 5423–5426, 2000.

[5] K. J. Puttlitz, and G. T. Galyon, "Impact of the ROHS directive on high-performance electronic systems," *Lead-Free Electronic Solders*, Springer, 2006, pp. 347–365.

[6] T. Takenaka, K-i. Maruyama, and K. Sakata, "$(Bi_{1/2}Na_{1/2})TiO_3$-$BaTiO_3$ system for lead-free piezoelectric ceramics," *The Japan Society of Applied Physis*, vol. 30, no. 9S, p. 2236, 1991.

[7] Y. Saito, H. Takao, T. Tani, T. Nonoyama, K. Takatori, T. Homma, T. Nagaya, and M. Nakamura, "Lead-free piezoceramics," *Nature*, vol. 432, no. 7013, pp. 84–87, 2004.

[8] T. Takenaka, K. M. K. Maruyama, and K. S. K. Sakata, "$(Bi_{1/2}Na_{1/2})TiO_3$-$BaTiO_3$ system for lead-free piezoelectric ceramics," *Japanese Journal of Applied Physis.*, vol. 30, no. 9S, p. 2236, 1991.

[9] M. Benyoussef, M. Zannen, J. Belhadi, B. Manoun, J.-L. Dellis, M. El. Marssi, and A. Lahmar, "Dielectric, ferroelectric, and energy storage properties in dysprosium doped sodium bismuth titanate ceramics," *Ceramics International*, vol. 44, no. 16, pp. 19451–19460, 2018.

[10] Y. Hiruma, H. Nagata, and T. Takenaka, "Thermal depoling process and piezoelectric properties of bismuth sodium titanate ceramics," *Journal of Applied Physics*, vol. 105, no. 8, pp. 084112–084118, 2009.

[11] P. Gonnard, and M. Troccaz, "Dopant distribution between A and B sites in the PZT ceramics of type ABO_3," *Journal of Solid State Chemistry*, vol. 23, no. 3–4, pp. 321–326, 1978.

[12] F. Gao, X. Dong, C. Mao, W. Liu, H. Zhang, L. Yang, F. Cao, and G. Wang, "Energy-storage properties of $0.89Bi_{0.5}Na_{0.5}TiO_3$–$0.06BaTiO_3$–$0.05K_{0.5}Na_{0.5}NbO_3$ lead-free anti-ferroelectric ceramics," *Journal of the American Ceramic Society*, vol. 94, no. 12, pp. 4382–4386, 2011.

[13] L. Zheng, X. Yi, S. Zhang, W. Jiang, B. Yang, R. Zhang, and W. Cao, "Complete set of material constants of $0.95(Na_{0.5}Bi_{0.5})TiO_3$-$0.05BaTiO_3$ lead-free piezoelectric single crystal and the delineation of extrinsic contributions," *Applied Physics Letters*, vol. 103, no. 12, p. 122905, 2013.

[14] W. Jo, T. Granzow, E. Aulbach, J.Rodel, and D. Damjanovic, "Origin of the large strain response in $(K_{0.5}Na_{0.5})NbO_3$-modified

$(Bi_{0.5}Na_{0.5})TiO_3$–$BaTiO_3$ lead-free piezoceramics," *Journal of Applied Physics*, vol. 105, no. 9, p. 094102, 2009.

[15] M. R. Bafandeh, H.-S. Han, and J.-S. Lee, "Enhanced electric field induced strain in complex-ion Ga^{3+} and Ta^{5+}-doped 0.93 BNT-0.07BT piezoceramic," *Journal of Electroceramics*, vol. 47, no. 3, pp. 89–99, 2021.

[16] Y. Xu, X. Liu, G. Wang, X. Liu, and Y. Feng, "Antiferroelectricity in tantalum doped $(Bi_{0.5}Na_{0.5})_{0.94}Ba_{0.06}TiO_3$ lead-free ceramics," *Ceramics International*, vol. 42, no. 3, pp. 4313–4322, 2016.

[17] J. Hao, Z. J. Xu, R. Chu, W. Li, P. Fu, J. Du, and G. Li, "Structure evolution and electrostrictive properties in $(Bi_{0.5}Na_{0.5})_{0.94}Ba_{0.06}TiO_3$–$M_2O_5$ (M= Nb, Ta, Sb) lead-free piezoceramics," *Journal of the European Ceramic Society*, vol. 36, no. 16, pp. 4003–4014, 2016.

[18] R. Zuo, C. Ye, X. Fang, and J. Li, "Tantalum doped $0.94Bi_{0.5}Na_{0.5}TiO_3$–$0.06BaTiO_3$ piezoelectric ceramics," *Journal of the European Ceramic Society*, vol. 28, no. 4, pp. 871–877, 2008.

[19] R. D. Shannon, "Revised effective ionic radii and systematic studies of interatomic distances in halides and chalcogenides," *Acta Crystallographica Section A*, vol. 32, no. 5, pp. 751–767, 1976.

[20] R. A. Malik, A. Hussain, A. Maqbool, A. Zaman, T. k. Song, W.-J. kim, and M.-H. Kim, "Giant strain, thermally-stable high energy storage properties and structural evolution of Bi-based lead-free piezoceramics," *Journal of Alloys and Compounds*, vol. 682, pp. 302–310, 2016.

[21] X. Qiao, F. Zhang, D. Wu, B. Chen, X. Zhao, Z. Peng, X. Ren, P. Liang, X. Chao, and Z. Yang, "Superior comprehensive energy storage properties in $Bi_{0.5}Na_{0.5}TiO_3$-based relaxor ferroelectric ceramics," *Chemical Engineering Journal*, vol. 388, p. 124158, 2020.

[22] P. Fu, Z. Xu, R. Chu, W. Li, G. Zang, and J. Hao, "Piezoelectric, ferroelectric and dielectric properties of La_2O_3-doped $(Bi_{0.5}Na_{0.5})_{0.94}Ba_{0.06}TiO_3$ lead-free ceramics," *Materials & Design*, vol. 31, no. 2, pp. 796–801, 2010.

[23] A. Ullah, Z. Yao, H. Liu, H. Hao, A. Manan, A. Ullah, A. Jan, M. Cao, S. Ahmad, and F. Alresheedi, "Improved energy storage properties of $La_{0.33}NbO_3$ modified $0.94Bi_{0.5}Na_{0.5}TiO_3$-0.06 $BaTiO_3$ ceramic system," *Applied Physics A*, vol. 127, pp. 1–12, 2021.

[24] P. Premwichit, T. Siritanon, W. Somsri, N. Nuntawong, O. Kosasang, S. Gupta, and S. Prasertpalichat "High energy-storage performance under low electric fields and enhanced electric-field-induced strain in Nb^{5+} doped BNT− BT lead-free piezoceramics," *Journal of Asian Ceramic Societies,* vol. 13, no. 1, pp. 154–168, 2025.

[25] W. Jo, S. Schaab, E. Sapper, L. A. Schmitt, H.-J. Kleebe, A. J. Bell, and J. Rodel, "On the phase identity and its thermal evolution of lead free $(Bi_{1/2}Na_{1/2})TiO_3$-6mol% $BaTiO_3$," *Journal of Applied Physics*, vol. 110, no. 7, p. 074106, 2011.

[26] P. Zhongbin, D. Hu, Y. Zhang, J. J. Liu, B. Shen, and J. Zhai, "Achieving high discharge energy density and efficiency with NBT-based ceramics for application in capacitors," *Journal of Materials, Chemistry C*, vol. 7, no. 14, pp. 4072–4078, 2019.

[27] X. Zhou, G. Xue, H. Luo, C. R. Bowen, and D. Zhang, "Phase structure and properties of sodium bismuth titanate lead-free piezoelectric ceramics," *Progress in Materials Science*, vol. 122, p. 100836, 2021.

[28] J. He, X. Liu, Y. Zhao, H. Du, T. Zhang, and J. Shi, "Dielectric stability and energy-storage performance of BNT-based relaxor ferroelectrics through Nb^{5+} and its excess modification," *ACS Applied Electronic Materials*, vol. 4, no. 2, pp. 735–743, 2022.

[29] Y. Yang, Z. Liu, P. Ren, Y. Mao, H. Sun, B. Liang, P. Mao, K. Guo, B. Xie, and L. Shu, "Modulation of phase boundary and domain structures to engineer strain properties in BNT-based ferroelectrics," *Journal of Advanced Ceramics*, vol. 13, no. 7, pp. 967–975, 2024.

[30] W. Zhou, T. Du, and C. Long, "High-efficiency lead-free bnt-based relaxor ferroelectrics via synergistic A/B-Site substitution for enhanced energy storage and stability," *Materials*, vol. 18, no. 23, p. 5259, 2025.

[31] P. Fu, Z. Xu, R. Chu, W. Li, G. Zang, and J. Jao, "Piezoelectric, ferroelectric and dielectric properties of Nd_2O_3-doped $(Bi_{0.5}Na_{0.5})_{0.94}Ba_{0.06}TiO_3$ lead-free ceramics," *Materials Science and Engineering B*, vol. 167, no. 3, pp. 161–166, 2010.

[32] J. Zang, M. Li, D. C. Sinclair, W. Jo, and J. Rodel, "Impedance spectroscopy of $(Bi_{1/2}Na_{1/2})TiO_3$–$BaTiO_3$ ceramics modified with $(K_{0.5}Na_{0.5})NbO_3$," *Journal of the American Ceramic Society*, vol. 97, no. 5, pp. 1523–1529, 2014.

[33] M. Chandrasekhar, D. K. Khatua, R. Pattanayak, and P. Kumar, "Dielectric relaxation and conduction mechanism studies of BNT-BT-BKT ceramics," *Journal of Physics and Chemistry of Solids*, vol. 111, pp. 160–166, 2017.

[34] F. Li, J. Zhai, B. Shen, X. Liu, and H. Zeng, "Simultaneously high-energy storage density and responsivity in quasi-hysteresis-free Mn-doped $Bi_{0.5}Na_{0.5}TiO_3$-$BaTiO_3$-$(Sr_{0.7}Bi_{0.2\square0.1})TiO_3$ ergodic relaxor ceramics," *Materials Research Letters*, vol. 6, no. 7, pp. 345–352, 2018.

[35] B. K. Barick, R. N. P. Choudhary, and D. K. Pradhan, "Dielectric and impedance spectroscopy of zirconium modified $(Na_{0.5}Bi_{0.5})TiO_3$ ceramics," *Ceramics International*, vol. 39, no. 5, pp. 5695–5704, 2013.

[36] H. Yanmin, D. Shi, L. Liu, G. Li, S. Zheng, and L. Fang, "High-temperature impedance spectroscopy of $BaFe_{0.5}Nb_{0.5}O_3$ ceramics doped with $Bi_{0.5}Na_{0.5}TiO_3$," *Applied Physics A*, vol. 114, no. 3, pp. 891–896, 2014.

[37] M. Li, M. J. Poetrowski, R. A. De. Souza, H. Zhang, I. M. Reaney, S. Cook, J. A. Kilner, and D. C. Sinclaie," A family of oxide ion conductors based on the ferroelectric perovskite $Na_{0.5}Bi_{0.5}TiO_3$," *Nature Materials*, vol. 13, no. 1, pp. 31–35, 2014.

[38] J. Shi, X. Liu, F. Zhu, W. Tian, Y. Xia, T. Li, R. Rao, T. Zhang, and L. Liu, "Oxygen vacancy migration and its lattice structural origin in A-site non-stoichiometric bismuth sodium titanate perovskites," *Journal of Materiomics*, vol. 8, no. 3, pp. 719–729, 2022.

[39] P. Premwichit, O. Kosasang, N. Triamnak, and S. Prasertpalichat, "Effects of Nd^{3+} donor doping on dielectric, electrical conductivity and ferroelectric properties of $(Bi_{0.5}Na_{0.5})_{0.93}Ba_{0.07}TiO_3$ lead-

free ceramics," *Integrated Ferroelectrics*, vol. 223, no. 1, pp. 185–195, 2021.

[40] J. Zuo, H. Yang, J. Chen, and C. Li, "Highly-reliable dielectric capacitors with excellent comprehensive energy-storage properties using $Bi_{0.5}Na_{0.5}TiO_3$-based relaxor ferroelectric ceramics," *Journal of the European Ceramic Society*, vol. 43, no. 6, pp. 2452–2459, 2023.

[41] W. Jo, R. Dittmer, M. Acosta, J. Zang, C. Groh, E. Sapper, K. Wang, and J. Rodel, "Giant electric-field-induced strains in lead-free ceramics for actuator applications–status and perspective," *Journal of Electroceramics*, vol. 29, no. 1, pp. 71–93, 2012.

[42] C. L. Freeman, J. A. Dawson, H.-R. Chen, J. H. Harding, L.-B. Ben, and D. C. Sinclair "A new potential model for barium titanate and its implications for rare-earth doping," *Journal of Materials Chemistry*, vol. 21, no. 13, pp. 4861–4868, 2011.

[43] M. Cernea, L. Trupina, C. Dragoi, B. S. Vasile, and R. Trusca, "Structural and piezoelectric characteristics of BNT–BT0.05 thin films processed by sol–gel technique," *Journal of Alloys and Compounds*, vol. 515, pp. 166–170, 2012.

[44] M. Cernea, A. C. Galca, M. C. Cioangher, C. Dragoi, and G. Loncea, "Piezoelectric BNT-BT0.11 thin films processed by sol–gel technique," *Journal of Materials Science*, vol. 46, no. 17, pp. 5621–5627, 2011.

[45] Y. Lan, C. Yuan, X. Liu, B. Zhu, L. Meng, C. Zhou, F. Liu, J. Xu, J. Wang, and G. Rao, "Semiconducting tailoring and electrical properties of A-site Co substituted $Bi_{0\cdot5}Na_{0\cdot5}TiO_{3-\delta}$ ferroelectric ceramics," *Materials Chemistry and Physics*, vol. 260, p. 124100, 2021.

[46] M. Wang, Q. Feng, C. Luo, Y. Ian, C. Yuan, N. Luo, C. Zhou, T. Fujita, J. Xu, G.-h. Chen, and Y. Wei, "Ultrahigh energy storage density and efficiency in $Bi_{0.5}Na_{0.5}TiO_3$-based ceramics via the domain and bandgap engineering," *ACS Applied Materials & Interfaces*, vol. 13, no. 43, pp. 51218–51229, 2021.

[47] J. Y. Tsao, S. Chowdhury, M. A. Hollis, D. Jena, N. M. Johnson, K. A. Jones, R. J. Kaplar, S. Rajan, C. G. Van de Walle, E. Bellotti, C. L. Chua, R. Collazo, M. E. Coltrin, J. A. Cooper, K. R. Evans, S. Graham, T. A. Grotjohn, E. R. Heller, M. Higashiwaki, M. S. Islam, P. W. Juodawlkis, M. A. Khan, A. D. Koehler, J. H. Leach, U. K. Mishra, Robert Nemanich, R. C.N. Pilawa-Podgurski, J. B. Shealy, Z. Sitar, M. J. Tadjer, A. F. Witulski, M. Wraback, and J. A. Simmons "Ultrawide-bandgap semiconductors: research opportunities and challenges," *Advanced Electronic Materials*, vol. 4, no. 1, p. 1600501, 2018.

[48] V. Palankovski, G. Kaiblinger-Grujin, and S. Selberherr, "Study of dopant-dependent band gap narrowing in compound semiconductor devices," *Materials Science and Engineering: B*, vol. 66, no. 1–3, pp. 46–49, 1999.

[49] R. K. Sahu, K. Banerjee, and S. Asthana, "Ergodic-nonergodic relaxor behavior, recoverable energy storage density, and dynamic hysteresis scaling in NKBT ferroelectrics," *Journal of Materials Science: Materials in Electronics*, vol. 34, no. 11, p. 972, 2023.

[50] A. Ullah, C. W. Ahn, A. Ullah, and I. W. Kim, "Large strain under a low electric field in lead-free bismuth-based piezoelectrics," *Applied Physics Letters*, vol. 103, no. 2, 2013.

[51] P. Premwichit, S. Jaila, and S. Prasertpalichat, "Effect of lanthanum doping on phase transition, piezoelectric and energy storage properties of lead-free $0.93(Bi_{0.5}Na_{0.5})TiO_3$–$0.07\ BaTiO_3$ ceramics," *Journal of Metals Materials and Minerals*, vol. 35, no. 4, p. e2358, 2025.

[52] J. Tangsritrakul, C. Wichittanankom, and C. Saiyasombat, "Composition-driven phase coexistence and functional properties of the (1-*x*)BZT-(*x*)BCT ceramics near the phase convergence region," *Journal of Metals Materials and Minerals*, vol. 34, no. 1, pp. 1798–1798, 2024.

[53] S. Pang, L. Yang, J. Qin, H. Qin, H. Xie, H. Wang, C. Zhou, and J. Xu, "Low electric field-induced strain and large improvement in energy density of $(Lu_{0.5}Nb_{0.5})^{4+}$ complex-ions doped BNT–BT ceramics," *Applied Physics A*, vol. 125, pp. 1–12, 2019.

[54] X. Liu, J. Zhai, B. Shen, F. Li, Y. Zhang, P. Li, and B. liu, "Electric-field-temperature phase diagram and electromechanical properties in lead-free $(Na_{0.5}Bi_{0.5})TiO_3$-based incipient piezoelectric ceramics," *Journal of the European Ceramic Society*, vol. 37, no. 4, pp. 1437–1447, 2017.

[55] R. A. Malik, A. Hussain, A. Zaman, A. Maqbool, J. Ur, Rahman, T. K. Song, W.-J. Kim, and M.-H. Kim, "Structure–property relationship in lead-free A-and B-site co-doped $Bi_{0.5}(Na_{0.84}K_{0.16})_{0.5}TiO_3$–$SrTiO_3$ incipient piezoceramics," *RSC Advances*, vol. 5, no. 117, pp. 96953–96964, 2015.